IMAGE SEGMENTATION BASED ON THE STATISTICAL VARIATIONAL FORMULATION USING THE LOCAL REGION INFORMATION

SUNG HA PARK[1], CHANG-OCK LEE[1†], AND JOOYOUNG HAHN[2]

[1]DEPARTMENT OF MATHEMATICAL SCIENCES, KAIST, DAEJEON 305-701, KOREA
E-mail address: colee@kaist.edu

[2]ADVANCED SIMULATION TECHNOLOGIES, AVL, GRAZ 8010, AUSTRIA

ABSTRACT. We propose a variational segmentation model based on statistical information of intensities in an image. The model consists of both a local region-based energy and a global region-based energy in order to handle misclassification which happens in a typical statistical variational model with an assumption that an image is a mixture of two Gaussian distributions. We find local ambiguous regions where misclassification might happen due to a small difference between two Gaussian distributions. Based on statistical information restricted to the local ambiguous regions, we design a local region-based energy in order to reduce the misclassification. We suggest an algorithm to avoid the difficulty of the Euler-Lagrange equations of the proposed variational model.

1. INTRODUCTION

Segmentation has been widely studied in the field of image processing and computer vision. It basically separates an image into several homogeneous regions according to a criterion. The quality of segmentation is crucial in other fields of image analysis such as motion tracking and image classification. Methods of segmentation are classified into two categories; one is the boundary-based segmentation which uses gradient information of an image to detect abrupt changes in the image and the other is the region-based segmentation which uses similarity information of an image to separate the image into several regions.

As basic boundary-based segmentations, there are filters by Roberts, Prewitt, Sobel [1, 2], and Canny [3]. These filters have a problem of irregularity of a curve which detects a boundary of an object in an image. Recently based on active contours models [4], variational formulations on deformable curves have been developed in order to handle the irregularity problem. These models consider energy functionals which consist of smoothness and attraction of a

curve. The energy for attraction of the curve commonly introduces an edge-detector function which makes a curve evolution converge at a boundary of an object as a minimizer of the energy functional. More advanced methods have been suggested in geometric active contours [5], geodesic active contours [6], and gradient vector flows [7]. With the help of the level set method [8, 9], these methods are able to deal with topological change which is a problem in the parametric deformable model [4]. However, there still remains a problem to capture weak boundaries changed smoothly from strong boundaries because these methods depend on edge-detector functions.

As region-based segmentations, there are thresholding, region growing [10], active contours without edges [11], and region competition [12]. Whereas the gradient-based segmentation uses local information on a deformable curve, the region-based segmentation uses global information of an image. In other words, an energy functional of the latter is formed by statistical information such as means and standard deviations of intensities on a region inside a deformable curve and a region outside the curve. Region competition [12] has been a fundamental framework in the region-based segmentation with an assumption that a given image is a mixture of two Gaussian distributions. Many region-based segmentations with the assumption have a problem of misclassification due to a small difference between two Gaussian distributions. The misclassification easily happens when an object has various intensities inside the boundary of the object or outside the boundary; see Figure 1.

Combinations of the boundary-based segmentation and the region-based segmentation have been also studied. Geodesic active regions [13, 14] combines geodesic active contours [6] and region competition [12] in order to segment a texture in an image. Region-aided geometric snake [15] adds the region force term in the geodesic active contours [6]. The region force is obtained from any region-based segmentation such as mean shift algorithm [16].

In this paper we propose a variational model based on statistical information of intensities in an image. The model consists of both a global region-based energy and a local region-based energy. The former roughly captures outlines of objects which we want to segment in an image. The latter reduces misclassification which happens in a typical statistical variational model with an assumption that the image is a mixture of two Gaussian distributions. We find local ambiguous regions where the misclassification happens due to small difference between two Gaussian distributions. Using statistical information restricted to the local ambiguous regions, we design the local region-based energy in order to reduce misclassification. We suggest an algorithm to avoid the difficulty of the Euler-Lagrange equations of the proposed energy functional.

The outline of this paper is as follows. In Section 2, we review the region competition and show what misclassification is in an image. In Section 3, we propose a statistical variational model and suggest an algorithm for segmentation. In Section 4, we show examples and comment numerical aspects of the algorithm. This paper is concluded in Section 5.

2. Region competition

Let Ω be a bounded closed subset of $\mathbf{R}^2$ and $I \colon \Omega \subset \mathbf{R}^2 \to \mathbf{R}$ be an image. A segmentation problem is to partition the image into several subregions which are characterized by prescribed properties. We assume that the image consists of two disjoint regions, i.e., $\Omega = \mathcal{R}_A \cup \mathcal{R}_B$ and intensities in the regions follow Gaussian distributions with probability density functions (PDFs) $\mathcal{P}(I; \alpha_i)$, $i \in \{A, B\}$, where $\alpha_i = (\mu_i, \sigma_i)$ is a Gaussian parameter of a mean μ_i and a standard deviation σ_i:

$$\mathcal{P}(I(x); \alpha_i) = \frac{1}{\sqrt{2\pi}\sigma_i} \exp\left(-\frac{(I(x) - \mu_i)^2}{2\sigma_i^2} \right).$$

Let Γ be the boundary separating two regions $\mathcal{R}_A$ and $\mathcal{R}_B$ and $\alpha = (\alpha_A, \alpha_B)$ be Gaussian parameters of two regions. Many energy functionals in typical statistical variational models [12–14] contain an energy term

$$E(\Gamma, \alpha) = - \sum_{i \in \{A, B\}} \int_{\mathcal{R}_i} \log \mathcal{P}(I(x); \alpha_i) dx, \qquad (2.1)$$

which generates a region competition as the energy is decreased.

In order to find a minimizer of the energy functional (2.1), an algorithm which consists of two alternating steps was used in [12]. In the first step, when a boundary Γ is fixed, the functional has a minimum if $\alpha_i = (\mu_i, \sigma_i)$ is the Gaussian parameter of the region $\mathcal{R}_i$:

$$\mu_i = \frac{1}{|\mathcal{R}_i|} \int_{\mathcal{R}_i} I(x) dx \quad \text{and} \quad \sigma_i^2 = \frac{1}{|\mathcal{R}_i|} \int_{\mathcal{R}_i} (I(x) - \mu_i)^2 dx$$

for $i \in \{A, B\}$. In the second step, when α is fixed, the Euler-Lagrange equation with respect to Γ is deduced and the gradient descent method is used. That is, the energy has a minimum if Γ is a curve C that is a steady state solution of

$$\frac{\partial C(x, t)}{\partial t} = F(x)\vec{n}, \quad F(x) = \log \mathcal{P}(I(x); \alpha_A) - \log \mathcal{P}(I(x); \alpha_B), \qquad (2.2)$$

where $\vec{n}$ is the outward normal vector to the curve(We assume that $\mathcal{R}_A$ is inside the curve C).

The evolution of the curve is generated by the sign of the force (2.2). The sign indicates that a point on the curve is more likely included into one of two regions $\mathcal{R}_A$ and $\mathcal{R}_B$. If $F > 0$ at a point, then the curve at the point moves along $\vec{n}$. It means that the point belongs to the region $\mathcal{R}_A$. If $F < 0$ at a point, on the other hand, the curve at the point moves along $-\vec{n}$ and the point belongs to the region $\mathcal{R}_B$. In this way, all points on the boundary belong to one of two regions. This process is called "region competition".

Unfortunately the region competition process may cause a problem which we call "misclassification". In Figure 1-(a), a minimizer of the energy functional (2.1) clearly captures the cross shape in the image. However, if an illumination is changed inside and outside the object in Figure 1-(c), a minimizer of the functional does not capture the cross shape. The reason is that some points whose intensities are near an intersection of two Gaussian PDFs are classified into a wrong region. That is, points whose intensities are near the intersection I^* in Figure 1-(d)
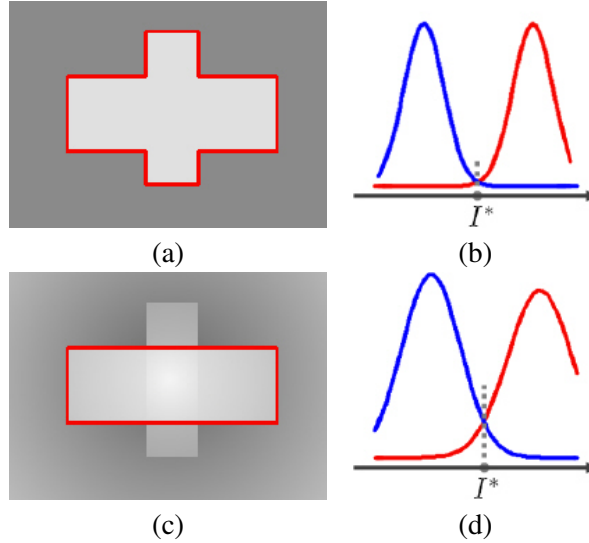
FIGURE 1. Red curves in (a) and (c) are minimizers of (2.1). Graphs in (b) and (d) are Gaussian PDFs when (2.1) is minimized. If an object and its background have simple colors, a minimizer of (2.1) clearly finds the object in an image. However, if an illumination is changed in the image, misclassification may happen where intensities are near the intersection I^* in (d).

are possibly misclassified in segmentation. We call the region which consists of such points as "local ambiguous region". In [12], in order to reduce misclassification, an energy functional was constructed using an average probability inside a window around points in an image. The algorithm to minimize the energy functional has a drawback that it is difficult to measure an optimal size of an window to obtain proper segmentation. It is also hard to decide how many seed points are needed in order to obtain computational efficiency. In this paper, we propose a variational model which overcome those drawbacks. The main purpose of the model is to handle misclassification in the local ambiguous regions.

3. STATISTICAL VARIATIONAL FORMULATION

3.1. **Modeling of energy functional.** Let Γ be a boundary separating two regions $\mathcal{R}_A$ and $\mathcal{R}_B$ and $\alpha = (\alpha_A, \alpha_B)$ be Gaussian parameters of two regions. Figure 1 tells us that if a difference of two Gaussian PDFs is large at a point, there is no misclassification when we classify the point according to the difference of Gaussian PDFs. However if the difference is small at a point, the classification of the point could be wrong. We define a set of such points as a local ambiguous region depending on Gaussian parameter α:

$$\mathcal{D}(\alpha) = \{x \mid H(f_\alpha(x)) = 1\}, \tag{3.1}$$

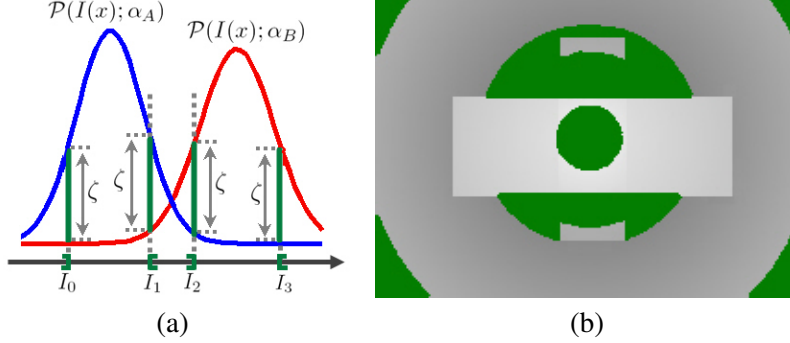(a)   (b)

FIGURE 2. Two graphs in (a) are Gaussian PDFs on $\mathcal{R}_A$ and $\mathcal{R}_B$. There are three intervals $[I_{\min}, I_0]$, $[I_1, I_2]$, and $[I_3, I_{\max}]$, where the difference of two PDFs is less than $\zeta(\alpha)$ in (3.2). The local ambiguous region $\mathcal{D}(\alpha)$ in (b) is a set of points x whose intensities $I(x)$ lie in the intervals. Each connected component in $\mathcal{D}(\alpha)$ is painted with green color.

where H is the Heaviside function,

$$f_\alpha(x) \equiv \zeta(\alpha) - |\mathcal{P}(I(x); \alpha_A) - \mathcal{P}(I(x); \alpha_B)|, \tag{3.2}$$

and $\zeta(\alpha)$ will be determined in Section 4.1. In Figure 2, (a) shows two Gaussian PDFs and three intervals $[I_{\min}, I_0]$, $[I_1, I_2]$, and $[I_3, I_{\max}]$, where the difference of PDFs is less than $\zeta(\alpha)$. Here $I_{\min}$ and $I_{\max}$ are the smallest intensity and the largest intensity in the image. Then the pixels whose intensities are in the intervals belong to the local ambiguous region. In (b), we depict the local ambiguous regions for Figure 1-(c) with green color.

Now, we propose a variational model which reduces misclassification in the local ambiguous region $\mathcal{D}(\alpha)$:

$$E(\Gamma, \alpha, \alpha^l) = - \sum_{i \in \{A,B\}} \left[\int_{\mathcal{R}_i \setminus \mathcal{D}(\alpha)} \log \mathcal{P}(I(x); \alpha_i) dx \right.$$
$$\left. + \int_{\mathcal{R}_i \cap \mathcal{D}(\alpha)} \log \mathcal{P}(I(x); \alpha_i^l) dx \right], \tag{3.3}$$

where $\alpha = (\alpha_A, \alpha_B)$ and $\alpha^l = (\alpha_A^l, \alpha_B^l)$. For a simple explanation, we assume that $\mathcal{D}(\alpha)$ is a connected subset of Ω. In practice, we consider different parameters α^l on each connected component of $\mathcal{D}(\alpha)$. The first term in (3.3) which we call the global region-based energy is the same as one in the model (2.1) except that the energy is contributed in the region $\mathcal{R}_i \setminus \mathcal{D}(\alpha)$ where a difference of two PDFs is large. In most cases, this term plays a dominant role to segment an outline of objects in an image. The second term which we call the local region-based energy is defined on the local ambiguous region $\mathcal{R}_i \cap \mathcal{D}(\alpha)$ where the difference is small. Whereas the global Gaussian parameter α_i makes a misclassification in $\mathcal{D}(\alpha)$, the local

Gaussian parameter α_i^l reduces the misclassification because α_i^l is obtained on not a global region $\mathcal{R}_A$ or $\mathcal{R}_B$, but a local region $\mathcal{R}_A \cap \mathcal{D}(\alpha)$ or $\mathcal{R}_B \cap \mathcal{D}(\alpha)$.

In order to find Euler-Lagrange equations for each variable, we write the proposed energy functional (3.3) using the function f_α in (3.2):

$$E(\Gamma, \alpha, \alpha^l) = - \sum_{i \in \{A,B\}} \int_{\mathcal{R}_i} \Big[H(f_\alpha) \log \mathcal{P}(I(x); \alpha_i^l)$$
$$+ \big(1 - H(f_\alpha)\big) \log \mathcal{P}(I(x); \alpha_i) \Big] \, dx.$$

First, we consider the minimization of the energy with respect to the boundary Γ. Fixing α and α^l, the Euler-Lagrange equation for Γ becomes

$$- \Big[H(f_\alpha) \big(\log \mathcal{P}(I(x); \alpha_A^l) - \log \mathcal{P}(I(x); \alpha_B^l) \big)$$
$$+ \big(1 - H(f_\alpha) \big) \big(\log \mathcal{P}(I(x); \alpha_A) - \log \mathcal{P}(I(x); \alpha_B) \big) \Big] \vec{n} = 0,$$

where $x \in \Gamma$. When the boundary Γ and α are fixed, the Euler-Lagrange equation for $\alpha^l = (\alpha_A^l, \alpha_B^l) = (\mu_A^l, \sigma_A^l, \mu_B^l, \sigma_B^l)$ produces the Gaussian parameter for intensities in regions indicated by $H(f_\alpha)$:

$$\mu_i^l = \frac{\displaystyle\int_{\mathcal{R}_i} H(f_\alpha) I(x) dx}{\displaystyle\int_{\mathcal{R}_i} H(f_\alpha) dx} \quad \text{and} \quad (\sigma_i^l)^2 = \frac{\displaystyle\int_{\mathcal{R}_i} H(f_\alpha)(I(x) - \mu_i^l)^2 dx}{\displaystyle\int_{\mathcal{R}_i} H(f_\alpha) dx}$$

for $i \in \{A, B\}$.

Finally fixing the boundary Γ and α^l, we consider the minimization of the energy with respect to the parameter $\alpha = (\mu_A, \sigma_A, \mu_B, \sigma_B)$. The necessary condition $\frac{\partial E}{\partial \mu_k} = 0$, $k \in \{A, B\}$ gives the equations

$$\sum_{i \in \{A,B\}} \int_{\mathcal{R}_i} H'(f_\alpha) \frac{\partial f_\alpha}{\partial \mu_k} \Big(\log \mathcal{P}(I(x); \alpha_i) - \log \mathcal{P}(I(x); \alpha_i^l) \Big) dx$$
$$- \int_{\mathcal{R}_k} \big(1 - H(f_\alpha) \big) \frac{I(x) - \mu_k}{\sigma_k^2} dx = 0. \tag{3.4}$$

The condition $\frac{\partial E}{\partial \sigma_k} = 0$, $k \in \{A, B\}$ gives the equations

$$\sum_{i \in \{A,B\}} \int_{\mathcal{R}_i} H'(f_\alpha) \frac{\partial f_\alpha}{\partial \sigma_k} \Big(\log \mathcal{P}(I(x); \alpha_i) - \log \mathcal{P}(I(x); \alpha_i^l) \Big) dx$$
$$- \int_{\mathcal{R}_k} \big(1 - H(f_\alpha) \big) \left(-\frac{1}{\sigma_k} + \frac{(I(x) - \mu_k)^2}{\sigma_k^3} \right) dx = 0. \tag{3.5}$$

Unfortunately, solving the equations (3.4) and (3.5) is not possible and what is worse, the parameter α is not relevant to Gaussian parameters on $\mathcal{R}_A$ and $\mathcal{R}_B$. The main problem comes from the fact that the local ambiguous region $\mathcal{D}(\alpha)$ in (3.1) depends on the parameter α.

3.2. **Modification of Euler-Lagrange equations.** In this section, we propose an algorithm to avoid the difficulty of Euler-Lagrange equations for α in (3.4) and (3.5). Since the difficulty comes from the dependence of the local ambiguous region on α in the proposed energy functional (3.3), to remove the dependence we regard $\mathcal{D}$ as a parameter in the functional

$$
\begin{aligned}
E(\Gamma, \mathcal{D}, \alpha, \alpha^l) = - \sum_{i \in \{A,B\}} \Bigg[& \int_{\mathcal{R}_i \setminus \mathcal{D}} \log \mathcal{P}(I(x); \alpha_i) dx \\
& + \int_{\mathcal{R}_i \cap \mathcal{D}} \log \mathcal{P}(I(x); \alpha_i^l) dx \Bigg].
\end{aligned}
\tag{3.6}
$$

However, we do not drop the dependence of $\mathcal{D}$ on α; we use (3.6) to find Euler-Lagrange equations with respect to α and $\mathcal{D}$ is determined by (3.1). Then we propose the following procedure

a) Initialize a curve Γ^n, $n = 0$.
b) Find regions $\mathcal{R}_A$ and $\mathcal{R}_B$ separated by the curve Γ^n and compute global Gaussian parameters α_A and α_B in each region:

$$
\mu_i = \frac{1}{|\mathcal{R}_i|} \int_{\mathcal{R}_i} I(x) dx \quad \text{and} \quad \sigma_i^2 = \frac{1}{|\mathcal{R}_i|} \int_{\mathcal{R}_i} (I(x) - \mu_i)^2 dx,
$$

for $i \in \{A, B\}$.
c) Determine the local ambiguous region $\mathcal{D}(\alpha)$ in (3.1).
d) Compute local Gaussian parameters α_A^l and α_B^l:

$$
\mu_i^l = \frac{1}{|\mathcal{D}_i|} \int_{\mathcal{D}_i} I(x) dx \quad \text{and} \quad (\sigma_i^l)^2 = \frac{1}{|\mathcal{D}_i|} \int_{\mathcal{D}_i} (I(x) - \mu_i^l)^2 dx,
$$

where $\mathcal{D}_i = \mathcal{R}_i \cap \mathcal{D}(\alpha)$ for $i \in \{A, B\}$.
e) Obtain the curve Γ^{n+1} by solving the equation

$$
\begin{aligned}
- \Big[& H(f_\alpha) \big(\log \mathcal{P}(I(x); \alpha_A^l) - \log \mathcal{P}(I(x); \alpha_B^l) \big) \\
& + \big(1 - H(f_\alpha) \big) \big(\log \mathcal{P}(I(x); \alpha_A) - \log \mathcal{P}(I(x); \alpha_B) \big) \Big] \vec{n} = 0.
\end{aligned}
\tag{3.7}
$$

f) If Γ^{n+1} is not changed from Γ^n, we stop the procedure. Otherwise, set $n = n + 1$ and repeat.

Note that the local ambiguous region $\mathcal{D}(\alpha)$ usually has many disjoint connected components, i.e., $\mathcal{D}(\alpha) = \bigcup_{k=1}^{N} \mathcal{D}^k$, $\mathcal{D}^i \cap \mathcal{D}^j = \emptyset$, $i \neq j$; see Figure 2.

Strictly speaking, the algorithm solves neither the Euler-Lagrange equations in Section 3.1 nor the variational model (2.1) on three different regions $\mathcal{R}_A$, $\mathcal{R}_B$ and $\mathcal{D}$. However, it keeps the main purpose of the proposed energy functional (3.3), which is to find the local ambiguous regions depending on the global Gaussian parameter α and to use the local Gaussian parameter

α^l to reduce misclassification. In the proposed algorithm, the parameter α represents statistical information on regions separated by the evolving curve Γ and the difficulty of Euler-Lagrange equations for α is avoided.

3.3. Extension to multi-dimensional Gaussian PDFs.
Our algorithm can be easily extended to multi-dimensional Gaussian PDFs which are used in a color image. The multi-dimensional Gaussian PDF is given by

$$\mathcal{P}(I(x)) = \frac{1}{2\pi^{\frac{d}{2}}|\Sigma|^{\frac{1}{2}}} \exp\left(-\frac{1}{2}(I(x) - \mu)^T \Sigma^{-1}(I(x) - \mu)\right), \tag{3.8}$$

where d is the number of channels and μ is the mean vector and Σ is the covariance matrix. Basically dealing with the RGB color model, we compute three dimensional probability density functions. If the channels are linearly dependent it is not possible to compute the PDF because $|\Sigma| = 0$ and hence Σ is not invertible in (3.8). To overcome the difficulty, we examine the correlation between channels to select independent channels. The correlation between two channels X, Y is given by

$$\rho_{XY} = \frac{Cov(X,Y)}{\sigma_X \sigma_Y},$$

where $Cov(X,Y)$ is the covariance of X, Y and σ_X, σ_Y are the standard deviations. If $|\rho_{XY}|$ is close to 1, X and Y are likely to be linearly dependent and if it is close to 0, they are almost linearly independent. Therefore if the correlation is larger than a criterion, then we take the average of two channels as one channel. Likewise we make a gray image if three channels are almost linearly dependent. Then two Gaussian PDFs $\mathcal{P}(I(x); \alpha_A)$ and $\mathcal{P}(I(x); \alpha_B)$ use the same channels.

4. NUMERICAL ASPECTS AND EXAMPLES

In this section, we raise numerical issues to solve (3.7) and show how to take a threshold $\zeta(\alpha)$ in (3.2).

4.1. Local ambiguous region.
In order to determine the local ambiguous region $\mathcal{D}(\alpha)$ in (3.1), we need to determine a criterion $\zeta(\alpha)$ in (3.2). The smaller the value $\zeta(\alpha)$ is, the smaller the region $\mathcal{D}(\alpha)$ becomes and the more dominant a global parameter α is in finding a boundary of an object in the proposed algorithm. Hence, the selection of $\zeta(\alpha)$ is crucial in our algorithm for segmentation.

Given a Gaussian PDF $\mathcal{P}(x)$ with a mean μ and $\eta(0 \leq \eta \leq 1)$, we first find β such that

$$\int_{\mu-\beta}^{\mu+\beta} \mathcal{P}(x)dx = \eta.$$

This means that the confidence interval of $100 \times \eta\%$ is $[\mu - \beta, \mu + \beta]$. Taking $\mathcal{P}(\mu + \beta)$ as a criterion, if $\mathcal{P}(x) < \mathcal{P}(\mu + \beta)$ at $x \in \Omega$, then we may regard the point x as an uncertain

point for classification. Based on this idea, we compute β_A and β_B for two Gaussian PDFs $\mathcal{P}(I(x); \alpha_A)$ and $\mathcal{P}(I(x); \alpha_B)$, respectively, in the proposed algorithm. Then we take

$$\zeta(\alpha_A, \alpha_B) = \min\{\mathcal{P}(\mu_A + \beta_A; \alpha_A), \mathcal{P}(\mu_B + \beta_B; \alpha_B)\}.$$

We used $\eta = 0.7$ for all examples.

4.2. **Evolution of the boundary.** With the gradient descent method and the level set method, (3.7) is formulated as

$$
\begin{aligned}
\frac{\partial \phi(x,t)}{\partial t} = &\Big[H(f_\alpha)\big(\log \mathcal{P}(I(x); \alpha_A^l) - \log \mathcal{P}(I(x); \alpha_B^l)\big) \\
&+ \big(1 - H(f_\alpha)\big)\big(\log \mathcal{P}(I(x); \alpha_A) - \log \mathcal{P}(I(x); \alpha_B)\big)\Big] |\nabla \phi(x,t)|,
\end{aligned}
\tag{4.1}
$$

where the zero level set of $\phi(x,t)$ is the evolving curve which separates two regions. Note that ϕ is a signed distance function with being positive inside the curve. The equation (4.1) may be solved numerically by the nonoscillatory scheme for space and the explicit Euler scheme for time [17] with ϕ^n as an initial curve. The numerical scheme, however, cause a severe restriction on the stability condition because the force is not bounded. Instead we find directly a steady state solution for the equation when the Gaussian parameters α and α^l are given. Since the steady state solution satisfies

$$F|\nabla \phi(x,t)| = 0$$

with F,

$$
\begin{aligned}
F = &H(f_\alpha)\big(\log \mathcal{P}(I(x); \alpha_A^l) - \log \mathcal{P}(I(x); \alpha_B^l)\big) \\
&+ \big(1 - H(f_\alpha)\big)\big(\log \mathcal{P}(I(x); \alpha_A) - \log \mathcal{P}(I(x); \alpha_B)\big)
\end{aligned}
$$

we simply take a step function

$$
\phi(x) = \begin{cases} 1 & \text{if } F(x) > 0, \\ -1 & \text{if } F(x) < 0, \\ 0 & \text{if } F(x) = 0, \end{cases} \quad \text{for } x \in \Omega
$$

and take the reinitialization process [18]. Then it becomes the solution ϕ^{n+1}.

4.3. **Examples.** In this section, we present several examples to illustrate our model and algorithm. We have two synthetic images on the top in Figure 3. These images are expected to have two modes, the object and the background. Note that two images have various intensities around boundaries of objects by illumination. We select the initial curve manually for each image as shown at the bottom in Figure 3. Figure 4 shows several iterates for two synthetic images when we apply our algorithm. For each image, local ambiguous regions are depicted by green color. In Figure 5 we compare our method with the region competition based on (2.1) and the Chan-Vese model in [11], which are most popular among the region-based segmentations. Figure 5-(a) is the results of two synthetic images when the region competition is applied, and (b) and (c) account for our model and the Chan-Vese model, respectively. Both (a) and (c) give

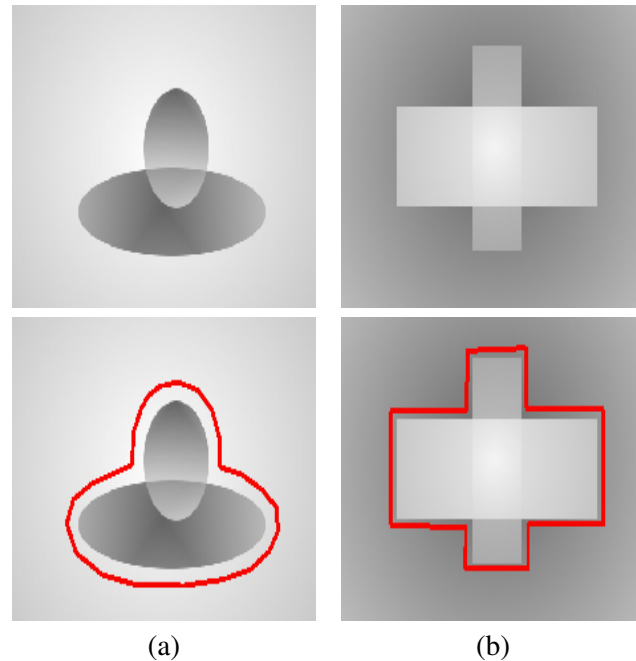(a)   (b)

FIGURE 3. Two synthetic images on the top and the initial curves at the bottom are shown. These images have various intensities around boundaries of objects by illumination.

wrong segmentation by passing though boundaries where illumination changes and these misclassification is inevitable, while our model gives exact boundary by reducing misclassification in ambiguous region as shown in Figure 4.

We apply our method to the real image taken in a studio. Figure 6-(a) is the original image where the object has various intensities inside the object as well as near its boundary, in particular, the top. The top is illuminated and forms weak edge. Notice that both sides of the object have highly concave parts. Thus the main problem for this image is to detect the weak edge and highly concave boundary simultaneously. With the same initial curve in Figure 6-(b), three models are applied; (c) is for the region competition, (d) and (e) are for our model and the Chan-Vese model, respectively. Three models detect correctly highly concave boundaries on both sides of the object. However, the region competition and Chan-Vese model fail to detect the weak edge on the top where the curves pass through the boundary of the object. On the other hand our model detects the weak edge correctly.

In Figure 7 there are three real images. Figure 7-(a) is a gray blurred noisy image, (b) is a shaded color image, and (c) is taken from the seashore with a digital camera. For three images we apply our method. In (d) numbers in the blurred noisy image are segmented without
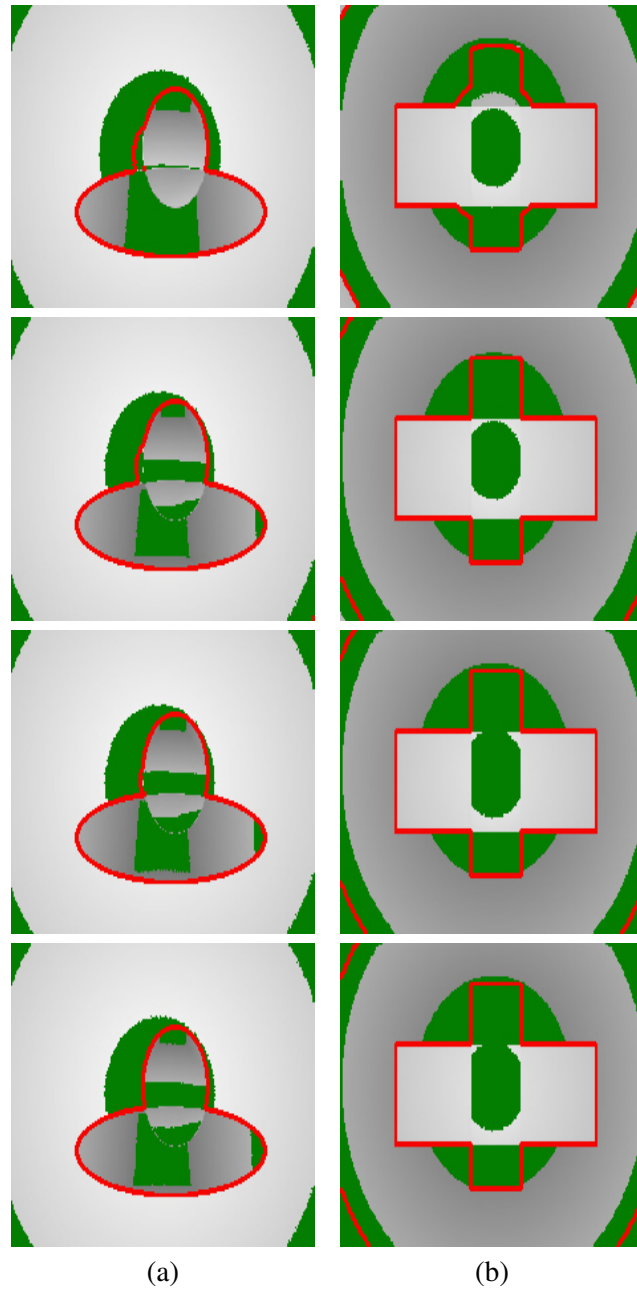
(a)   (b)

FIGURE 4. Several iterates are shown for two synthetic images when our method is applied. From the top to the bottom, $n = 1, 2, 3, 4$. For each image, local ambiguous regions are depicted by green color.

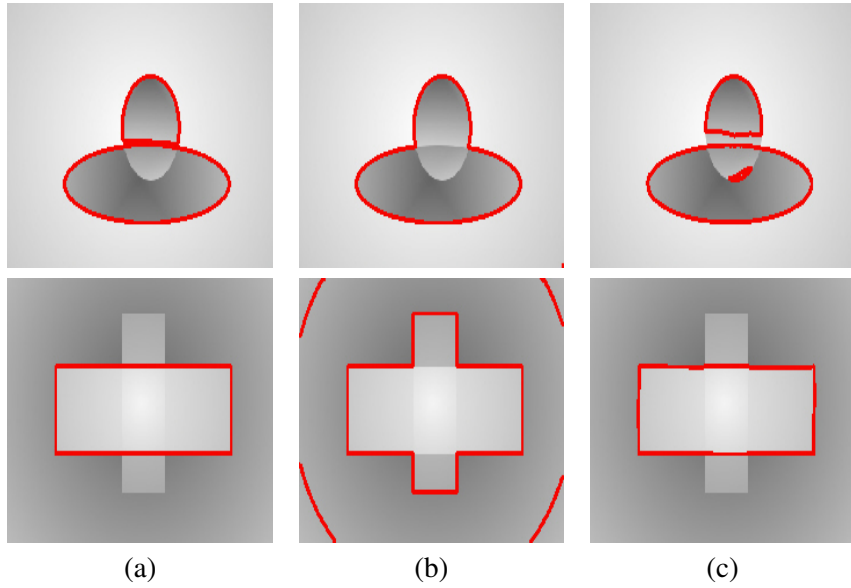(a)   (b)   (c)

FIGURE 5. For two synthetic images, three models are applied. (a) is obtained when the region competition is used and (b) is for our model and (c) is for the Chan-Vese model. Notice that (a) and (c) fail to detect boundaries correctly. On the other hand our model gives the correct boundary between the object and the background.

corruption of noise. Alphabet letters are separated from the background in (e). (f) shows segmentation between a boy and the sandy plain. The shadow near the boy is excluded.

5. CONCLUSIONS

In this paper we proposed a variational segmentation model based on statistical information of intensities in an image. Since the global region-based energy model which uses the statistical information in whole region causes misclassification, in order to reduce misclassifications, we defined the local ambiguous region, where the difference of two Gaussian PDFs is small and considered an energy using the local Gaussian parameter restricted to the local region. Then we combined the local region-based energy with the global region-based energy. This model, however, induces the difficulty in handling Euler-Lagrange equations. We thus proposed an algorithm to avoid the difficulty. It consists of several steps to solve Euler-Lagrange equations; the local ambiguous region as a parameter of the energy is determined explicitly after the global Gaussian parameters are computed. With several examples we confirmed that our model and the algorithm reduced misclassification and hence detected the boundary of the object when an illumination is changed.
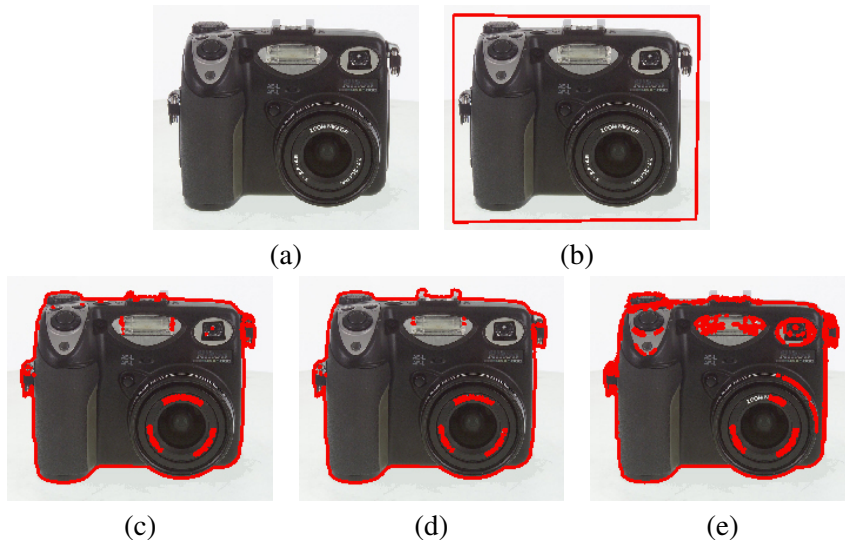
FIGURE 6. (a) is an image taken from a studio. It has weak boundary on the top as well as highly concave shape on the sides of the object. An initial curve(red line) is shown in (b). With this initial curve, three segmentation models are applied. Different results are shown at the bottom. (c) is obtained from the region competition, (d) is from our model, and (e) is from the Chan-Vese model. Our method detects both weak edge and highly concave shape.

REFERENCES

[1] R. C. Gonzalez and R. E. Woods. *Digital image processing*. Prentice-Hall, New Jersey, 2002.

[2] A. K. Jain. *Fundamentals of digitial image processing*. Prentice-Hall, New Jersey, 2003.

[3] J. Canny. A computational approach to edge detection. *IEEE Trans. Pattern Anal. Machine Intell.*, 8:679–698, 1986.

[4] M. Kass, A. Witkin, and D. Terzopoulos. Snakes: Active contour models. *Int. J. Comput. Vis.*, 1:321–331, 1988.

[5] V. Caselles, F. Catté, T. Coll, and F. Dibos. A geometric model for active contours in image processing. *Numer. Math.*, 66:1–31, 1993.

[6] V. Caselles, R. Kimmel, and G. Sapiro. Geodesic active contours. *Int. J. Comput. Vis.*, 22:61–79, 1997.

[7] C. Xu, A. Yezzi, and J. L. Prince. On the relationship between parametric and geometric active contours. *Proc. of 34th Asilomar Conference on Signals, Systems, and Computers*, 1:483–489, 2000.

[8] S. J. Osher and J. A. Sethian. Fronts propagating with curvature dependent speed: Algorithms based on Hamilton-Jacobi formulations. *J. Comput. Phys*, 79:12–49, 1988.

[9] J. A. Sethian. *Level set methods*. Cambridge University Press, New York, 1996.

[10] R. Adams and L. Bischof. Seeded region growing. *IEEE Trans. Pattern Anal. Machine Intell.*, 16:641–647, 1994.

[11] T. Chan and L. Vese. Active contours without edges. *IEEE Trans. Image Processing*, 10:266–277, 2001.

[12] S. C. Zhu and A. Yuille. Region competition: unifying snakes, regions growing, and Bayes/MDL for multi-band image segmentation. *IEEE Trans. Pattern Anal. Machine Intell.*, 18:884–900, 1996.
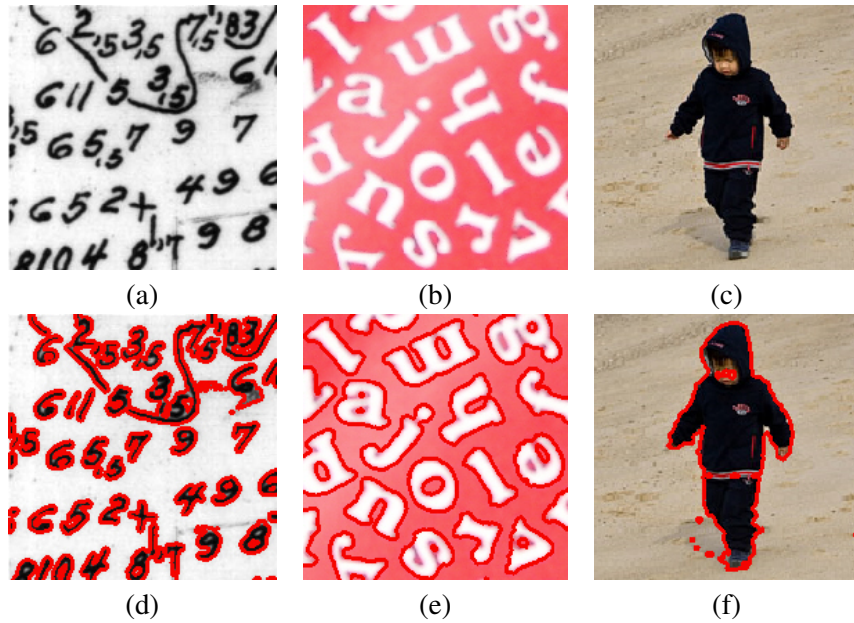
FIGURE 7. There are three real images on the top. (a) is a gray noisy image which is blurred. (b) is a shaded color image and (c) is taken from the seashore with a digital camera. Images at the bottom are the results of our algorithm.

[13] N. Paragios and R. Deriche. Geodesic active regions and level set methods for supervised texture segmentation. *Int. J. Comput. Vis.*, 46:223–247, 2002.

[14] N. Paragios and R. Deriche. Geodesic active regions: A new framework to deal with frame partition problems in computer vision. *J. Vis. Commun. and Image Represent.*, 13:249–268, 2002.

[15] X. Xie and M. Mirmehdi. RAGS: Region-aided geometric snake. *IEEE Trans. Image Processing*, 13:640–652, 2004.

[16] D. Comaniciu and P. Meer. Mean shift: A robust approach toward feature space analysis. *IEEE Trans. Pattern Anal. Machine Intell.*, 24:603–619, 2002.

[17] G. Aubert and P. Kornprobst. *Upwind differencing schemes for hyperbolic conservation laws with source terms*. Springer-Verlag, New York, 2002.

[18] M. Sussman, P. Smereka, and S. Osher. A level set approach for computing solutions to incompressible two-phase flow. *J. Comput. Phys.*, 114:146–159, 1994.